Title *Mafb* Deficiency in Myeloid Cells Increases Susceptibility to *Mycobacterium tuberculosis* Infection in Mice

Haruka Hikichi[1,2], Hajime Nakamura[1,2], Omori Shiho[1], Shintaro Seto[1], Minako Hijikata[1], Michito Hamada[3,4], Satoru Takahashi[3], Naoto Keicho[2,5]

[1]Department of Pathophysiology and Host Defense, The Research Institute of Tuberculosis, Japan Anti-Tuberculosis Association, Tokyo, Japan

[2]Department of Basic Mycobacteriosis, Nagasaki University Graduate School of Biomedical Sciences, Nagasaki, Japan

[3]Laboratory Animal Resource Center in Transborder Medical Research Center, and Department of Anatomy and Embryology, Institute of Medicine, University of Tsukuba, Ibaraki, Japan

[4]Center for Medical Sciences, Ibaraki Prefectural University of Health Sciences, Ibaraki, Japan

[5]Vice Director, The Research Institute of Tuberculosis, Japan Anti-Tuberculosis Association, Tokyo, Japan

Correspondence: Shintaro Seto

s-seto@jata.or.jp

Running title: Vulnerability to *Mtb* infection in *Mafb*-cKO mice

Keywords: MAFB, *Mycobacterium tuberculosis*, conditional knockout mouse, mRNA

25 sequencing, host defense

Abstract

v-Maf avian musculoaponeurotic fibrosarcoma oncogene homolog B (*MAFB*) is a candidate gene associated with early tuberculosis onset identified by a genome-wide association study. Here, we investigated the role of *Mafb* in susceptibility to *Mycobacterium tuberculosis* (*Mtb*) infection in myeloid-specific *Mafb*-knockout (*Mafb*-cKO) mice. We infected bone marrow-derived macrophages (BMMs) from *Mafb*-cKO mice and *Mafb*-cKO mice with *Mtb*. The absence of *Mafb* promoted *Mtb* proliferation in BMMs. RNA sequencing (RNA-seq) revealed activation of the metabolic process and impairment of the response to type I interferons (IFNs) in *Mtb*-infected BMMs from *Mafb*-cKO mice, which conforms to our previous findings in *Mtb*-infected human macrophages with *MAFB* knockdown. *Mafb* deficiency increased mortality and bacterial burden in the lungs and spleens during *Mtb* infection in mice. RNA-seq revealed weakened leukocyte or lymphocyte chemotaxis in *Mtb*-infected *Mafb*-cKO mouse lungs. Flow cytometry demonstrated an alteration in the proportion of immune cells in *Mtb*-infected mouse lungs due to *Mafb* deficiency. Together, *Mafb* in myeloid cells is involved not only in the functional antibacterial process of macrophages but also in immune cell recruitment in the lungs, thereby contributing to host defense against *Mtb* infection.

Introduction

Tuberculosis (TB), caused by *Mycobacterium tuberculosis* (*Mtb*) infection, has resurged as the leading infectious disease, with 8.2 million newly diagnosed cases and 1.2 million deaths in 2023 alone (1). The newly proposed spectrum of TB categorizes this disease into five stages based on the level of infectiousness, presenting symptoms, and macroscopic pathology (2). In this category, subclinical TB is accountable for half the TB burden in any community, making it potentially infectious without any symptoms (3). Therefore, early diagnosis, preventive therapy, or treatment of subclinical TB is critical to prevent further transmission and to ultimately achieve global TB elimination (4). Several studies have attempted to estimate the activation risk based on gene signatures or transcriptional biomarkers (5). Notably, it is important to investigate the factors that determine the trajectory of infection in TB patients or drive susceptibility to TB so as to understand this complex disease as well as to accelerate research in drug and vaccine development.

To date, numerous genome-wide association studies (GWASs) have been conducted to investigate the host genetic factors in TB susceptibility. However, only a few associations have proven reproducibility owing to the modest population sizes, variability in phenotyping across studies, population-specific effects, or complex population structures under certain high-burden settings (6). A meta-analysis combining two GWASs in Thai and Japanese populations did not replicate the association of 25 selected single-nucleotide polymorphisms (SNPs) (7). However, the age-stratified analysis from the same dataset revealed a significant locus on chromosome 20q12 linked to the younger onset group. This locus is located approximately 450-kb upstream of *v-maf avian musculoaponeurotic fibrosarcoma oncogene homolog B* (*MAFB*). Early-

69 onset of TB implies the relatively sooner development after exposure to *Mtb*. The
70 GWAS result suggests that *MAFB* plays a role in the host immunity toward controlling
71 *Mtb* infection. With this background, we investigated the role of *MAFB* as a promising
72 candidate gene involved in TB susceptibility.

73 MAFB belongs to the large Maf family of transcription factors characterized by
74 a conserved basic leucine zipper (bZip) enabling specific DNA binding to Maf-
75 recognition elements (MAREs) (8). *Mafb* was first identified as a causative gene for
76 segmentation abnormalities in the hindbrain and in defective inner ear development (9).
77 Lethal phenotypes observed in *Mafb*-null mice, including respiratory failure, renal
78 dysgenesis, and parathyroid abnormalities, indicate the critical role of *Mafb* in
79 organogenesis (10). *Mafb* has been demonstrated to control the expression of apoptosis
80 inhibitor of macrophages (AIM) and promote atherosclerosis through inhibiting foam-
81 cell apoptosis (11). In addition, *Mafb* plays diverse roles in various biological processes
82 (BPs), including the myeloid commitment of hematopoietic stem cells, self-renewal of
83 macrophages, generation of thymus, or the creation of hair cuticles (10).

84 In the context of immune regulation and infectious disease, *MAFB* has been
85 reported to control antiviral response and macrophage polarization (12, 13). Previously,
86 we investigated the function of *MAFB* in *Mtb*-infected human macrophages to explore
87 the biological mechanism underlying *MAFB* in macrophages (14). Our gene knockdown
88 (KD) experiments revealed that MAFB regulates the gene expression related to
89 interferon (IFN) responses in *Mtb*-infected macrophages. In the present study, we
90 investigated the role of *MAFB*, particularly in disease outcomes and dynamic immune
91 cell interactions in organisms by using myeloid-specific *Mafb*-knockout (*Mafb*-cKO)
92 mice (15). We monitored the survival and bacterial burden in the murine organs and

found that *Mafb*-cKO mice had higher mortality and bacterial burden during the *Mtb* infection. RNA sequencing (RNA-seq) of *Mtb*-infected *Mafb*-cKO mouse lungs revealed a disrupted chemotaxis. These results were consistent with altered immune cell populations in the lungs of *Mtb*-infected *Mafb*-cKO mice. Taken together, this study highlights *MAFB* as an important gene in macrophages that contributes to protective immunity against *Mtb* infection.

Materials and Methods

Ethics statement

Animal experiments in this study were approved by the Animal Care and Use Committee of the Research Institute of Tuberculosis (RIT) (permit number: No. 2021-04). Animals were treated in accordance with the ethical guidelines of RIT. The endpoints were set to determine whether the mice were imminently dying of *Mtb* infection and/or required compassionate euthanasia: bodyweight loss >20% of the initial bodyweight at the time of infection.

Mice

Macrophage-specific *Mafb* conditional-knockout (*Mafb*$^{f/f}$::LysM-Cre$^{+/+}$ or *Mafb*$^{f/f}$::LysM-Cre$^{+/-}$, *Mafb*-cKO) and *Mafb*$^{f/f}$ control mice were used (15). *Mafb*-cKO and control mice (*Mafb*$^{f/f}$) were maintained in a filtered-air laminar-flow cabinet and provided with sterile bedding, water, and mouse chow at an RIT animal facility. Wild-type (WT) C57BL/6J mice were obtained from The Jackson Laboratory Japan, Inc. Specific pathogen-free status was verified by testing sentinel mice housed within the colony.

117

118 ***Mtb* culture**

119 The *Mtb* strain Erdman was used and stored as previously described (16-18).
120 For determining the bacterial burden in macrophages, the infected cells were lysed with
121 PBS containing 0.1% SDS. Infected lungs or spleens were homogenized using a
122 ShakeMaster Neo (Bio Medical Science). The resulting cell lysates or homogenates
123 were serially diluted and plated in duplicate on 7H10 or 7H11 agar plates supplemented
124 with 10% Middlebrook OADC (BD Bioscience) and 0.5% glycerol. *Mtb* colony-
125 forming units (CFUs) were determined by calculating the mean CFU count from the
126 two plates at each dilution.

127

128 **Bone marrow-derived macrophage (BMM) isolation**

129 BMMs were differentiated as described previously (19), with some
130 modifications. Briefly, bone marrow was isolated from the hind legs of *Mafb*-cKO and
131 control mice (6 weeks), washed, and suspended into a single cell by passing through a
132 cell strainer. The bone marrow cells were then incubated at a concentration of 2×10^6
133 cells/mL in DMEM (Sigma-Aldrich) supplemented with 10% inactivated-fetal bovine
134 serum (FBS, JRH Biosciences Inc.) and 10% of L929-conditioned medium in a 12-well
135 plate for 7 days. Differentiated macrophages in DMEM containing 10% FBS were
136 infected with *Mtb* at a multiplicity of infection (MOI) of one. At one day postinfection
137 (p.i.), BMMs were collected for mRNA sequencing (mRNA-seq). At 1, 3, and 7 days
138 p.i., the number of the intracellular bacteria within BMMs was determined by CFU.

139

140 ***Mtb* infection in mice**

141 The experimental mice (age: 6–10 weeks) were transferred to a biosafety level
142 3 animal facility at RIT. The mice were infected with *Mtb* via the aerosol route using an
143 inhalation exposure system (Glas-Col). This method routinely gave *Mtb* infection at
144 100–200 CFU per lung one day p.i.
145
146 **Survival study**
147 WT and *Mafb*-cKO mice infected with *Mtb* were monitored for 315 days. The
148 mice that survived throughout the experiments or met the endpoint were euthanized by
149 exsanguination under anesthesia with 0.75 mg/kg of medetomidine, 4.0 mg/kg of
150 midazolam, and 5.0 mg/kg of butorphanol *via* the intraperitoneal route (20). Survival
151 probabilities between the two groups were analyzed using Kaplan–Meier analysis and
152 the log-rank test.
153
154 **mRNA-seq**
155 mRNA-seq was performed as described previously (18). Briefly, infected
156 BMMs or lungs were homogenized with TRIzol Reagent (Invitrogen), followed by
157 RNA purification using an RNeasy Mini kit (Qiagen). Total RNA qualified and
158 quantified by a 4150 TapeStation system (Agilent) and a Qubit 4 Fluorometer
159 (Invitrogen), respectively, was subjected to construct cDNA libraries using NEBNext®
160 Poly(A) mRNA Magnetic Isolation Module (New England Biolabs) and NEB Next
161 Ultra™ II DNA Library Prep Kit for Illumina (New England Biolabs). All the cDNA
162 libraries were examined for quality using a 4150 TapeStation system and quantified
163 with a Qubit 4 Fluorometer. The libraries were sequenced with a NextSeq1000 system
164 (Illumina).

Data processing

For read-quality trimming, raw reads were processed with Trim Galore v0.6.7 (https://github.com/FelixKrueger/TrimGalore). The expressions of transcripts were estimated by Salmon v0.12.0 directly from the processed reads (21). Transcript-level expression data was then summarized into gene-level data by the R package tximport v1.30.0 (https://github.com/thelovelab/tximport) in R v4.3.3(22). The analysis for differentially expressed genes (DEGs) was performed by edgeR v4.0.16 (23) using generalized linear models and quasi-likelihood tests (24). The DEGs were further utilized to perform Gene Ontology (GO) enrichment analysis to identify enriched BPs using the R package clusterProfiler v4.10 (25). To reduce redundancy among the identified GO BP categories, a simplification method in clusterProfiler was used. The gene concept network of the top 3 upregulated and downregulated GOBP categories was visualized by cnetplot in clusterProfiler. KEGG pathway enrichment analysis was conducted using ShinyGO v0.82 (26), an online gene set enrichment tool (http://bioinformatics.sdstate.edu/go/). Adapted KEGG pathway diagrams were visualized using Pathview v1.42.0 in R software (27). Pathway source: KEGG (https://www.kegg.jp). Gene set enrichment analysis (GSEA) was performed locally using the GSEA desktop application (Broad Institute, v4.2.3) with the WikiPathway gene sets (c2.cp.wikipathways.v2024.1.Hs.symbols.gmt) obtained from the Molecular Signature Database (MSigDB). MafB ChIP-seq peaks (GEO GSM1964739/SRA SRX1465586) (28) were downloaded via ChIP-Atlas (accessed 27 June 2025) (29) and compared with the DEGs identified in the present study. The ChIP-seq Atlas is accessible at https://chip-atlas.org/.

189

190 **Flow cytometry**

191 Infected lung cells were obtained using the Lung Dissociation Kit (Miltenyi
192 Biotec) according to the manufacturer's instructions. Briefly, cell suspensions from the
193 lungs were incubated with ACK buffer to lyse red blood cells. The cells were washed
194 and diluted in MACS buffer (PBS supplemented with 2mM EDTA and 2% FBS) to
195 achieve 1–3 × 10^6 cells/mL. The cells were incubated with TruStain FcX™ PLUS (anti-
196 mouse CD16/32) (Biolegend), followed by staining with antibodies against CD4, CD8,
197 CD45R, CD3, SiglecF, CD64, CD11b, CD45, or Ly6G (BioLegend). The stained cells
198 were then fixed with the fixation buffer (BioLegend) to inactivate infected *Mtb* for 24 h
199 at 4°C. The cells were analyzed on a BD FACSLyric™ using analysis software BD
200 FACSuite™ Application V1.4.0.7047 and FlowJo™ Software v10.10 (BD Biosciences).

201

202 **Results**

203 ***Mafb* deficiency on mycobacterial killing in macrophages**

204 In our previous study, we demonstrated impaired inflammatory responses in
205 *MAFB* knockdown, PMA-stimulated THP-1 cells (*MAFB*-KD macrophages). However,
206 no significant difference in bacterial burden was observed between *MAFB*-KD
207 macrophages and control macrophages at 24 h or 48 h p.i., suggesting that the
208 knockdown effect and/or the duration of infection was insufficient to detect intracellular
209 bacterial proliferation (14). In this study, we investigated the effect of *Mafb* deficiency
210 on mycobacterial proliferation in BMMs (**Figure 1**). For this purpose, we infected
211 BMMs of *Mafb*$^{f/f}$::LysM-Cre$^{+/-}$ (*Mafb*-cKO) or *Mafb*$^{f/f}$ (control) with *Mtb* at an MOI of
212 one for 1, 3, and 7 days. At 3 and 7 days p.i., *Mafb*-cKO BMMs exhibited a higher

213 bacterial burden compared to control BMMs. Notably, the intracellular number of *Mtb*
214 in *Mafb*-cKO BMMs increased significantly more rapidly from day 3 to day 7,
215 suggesting that the absence of *Mafb* transforms macrophages into a more permissive
216 environment for *Mtb* proliferation.
217

218 ***Mafb*-cKO BMMs demonstrated functional changes in metabolic process and**
219 **immune response during *Mtb* infection**

220 When macrophages are exposed to *Mtb*, they internalize the bacteria, and *Mtb*
221 begins adapting to the intracellular environment by 24 h p.i. During this period,
222 macrophages undergo robust transcriptional changes, indicating active host–pathogen
223 interactions (30). To investigate the transcriptional function of *Mafb* in *Mtb*-infected
224 macrophages, we infected BMMs from *Mafb*$^{f/f}$::LysM-Cre$^{+/-}$ (*Mafb*-cKO) and *Mafb*$^{f/f}$
225 (control) with *Mtb* and conducted mRNA-seq at 24 h p.i. mRNA-seq comparing
226 between *Mtb*-infected BMMs from *Mafb*-cKO and control mice identified 1223 DEGs
227 (**Figure 2A**). GO analysis for BP (GOBP) identified 974 significantly enriched GOBP
228 terms in 614 upregulated DEGs in *Mtb*-infected *Mafb*-cKO BMMs, including leukocyte
229 cell–cell adhesion, reactive oxygen species (ROS) metabolic process, or nucleotide
230 metabolic process (**Figure 2B**). In 609 downregulated DEGs, 493 significantly enriched
231 GOBP terms were identified, including response to virus, defense response to symbiont,
232 or regulation of innate immune response (**Figure 2B**). To visualize the interactions of
233 the genes annotated to each GO term, we constructed gene networks (**Figure 2C**).
234 Upregulated genes annotated to leukocyte cell–cell adhesion include *Itgb2*, *Itgb7*, *Itgal*,
235 *F11r*, *Selplg*, *Cd44* (adhesion molecules or integrins), *Ccr2*, *Cx3cr1*, *Cd86*, *Cd74*,
236 *Cd24a*, *Cd177*, *Cd300a* (leukocyte surface receptors), *H2-Ab1*, *H2-Aa*, *H2-Eb1*, *H2-*

237 *DMa*, *H2-DMb1* (MHC molecules), and *Arg2*, *Thbs1*, *Alox5*, *Sirpb1b*, *Sirpb1c* (immune
238 modulation), suggesting that the macrophages are in the state where they are actively
239 participating in immune surveillance, cellular communication, and antigen presentation.
240 Genes annotated to ROS metabolic process include *Cybb*, *Cyba*, *Ncf2* (ROS
241 generation), *Prdx1*, *Prdx5*, *Prdx6*, *Txn1*, *Txnrd1*, *Sod2*, *G6pdx*, *Gpx3*, *Nnt* (ROS
242 detoxification, antioxidant defense), and *Thbs1*, *Rhoa*, *Atg5* (oxidative stress
243 modulation). The downregulated genes annotated to top significantly enriched GOBP
244 terms were highly overlapped: *Apobec1*, *Adar*, *Ifi204*, *Ifi203*, *Ifi205*, *Ifi206*, *Ifi207*,
245 *Ifi208*, *Ifi209*, *Ifi211* (RNA editing and modification), *Ifih1*, *Dhx58*, *Rigi*, *Ddx60*, *Stat1*,
246 *Stat2*, *Irf3*, *Irf7*, *Tbk1*, *Trim25*, *Trim5*, *Trim21*, *Trim30a*, *Trim30c*, *Trim30d*, *Trim34a*,
247 *Trim35*, *Trim12c*, *Trim8*, *Isg15*, *Isg20*, *Oas1a*, *Oas1g*, *Oas2*, *Oas3*, *Oasl2*, *Ifit1*, *Ifit2*,
248 *Ifit3*, *Ifit3b*, *Ifit1bl1*, *Mx1*, *Mx2*, *Bst2*, *Dtx3l*, *Rnasel*, *Parp9*, *Shfl*, *Slfn8*, *Slfn9*, *Gbp3*,
249 *Gbp5*, *Gbp7*, *Rnf135*, *Nt5c3* (innate immune sensors and IFN-stimulated genes (ISGs)),
250 *Irgm1*, *Irgm2*, *Igtp*, *Mov10* (autophagy and intracellular pathogen defense), *Pou2f2*,
251 *Il10rb*, *Il15*, *Tlr9*, *Tlr1*, *Cd37*, *Cd180*, *Cd36*, *Cd300ld3*, *Pik3ap1*, *Rtp4*, *Sash1*, *Trafd1*,
252 *Appl2* (transcription factors and signal transduction), *Eif2ak2*, *Pml*, *Bcl2l1*, *Trex1*, *Xaf1*,
253 *Htra2*, *F830016B08Rik* (cell cycle, apoptosis, and DNA repair), *Lacc1*, *Apoe*, *Adam8*,
254 and *Hyal1* (metabolism and miscellaneous functions). These downregulated DEGs
255 suggested weakened pathogen sensing and reduced IFN response or inflammatory
256 signaling, indicating a potential shift to an anti-inflammatory phenotype in *Mtb*-infected
257 BMMs of *Mafb*-cKO mice. KEGG pathway enrichment analysis revealed that oxidative
258 phosphorylation and chemical carcinogenesis-ROS were enriched in the upregulated
259 DEGs (**Supplementary Figure 1A**), whereas ECM-receptor interaction, lysosome, and
260 endocytosis were enriched in downregulated DEGs (**Supplementary Figure 1B**). As

261 depicted in the lysosome pathway diagram, the proton pump ATPeV, which plays a
262 critical role in lysosomal acidification, is downregulated (**Supplementary Figure 2)**
263 (31). By GSEA using all expressed genes, a pathway of immune response to TB
264 (https://www.wikipathways.org/instance/WP4197) exhibited impairment in *Mtb*-
265 infected *Mafb*-cKO BMMs (**Supplementary Figure 3**). These enriched BPs and
266 pathways are consistent with the previous results obtained from mRNA-seq of *Mtb*-
267 infected *MAFB*-KD macrophages (14). IFN-gamma inducible chemokines (*Cxcl11*,
268 *Ccl2*, *Ccl7*, *Cxcl9*, *Cxcl10*) were downregulated in *Mtb*-infected *MAFB*-KD
269 macrophages, as well as in *Mtb*-infected BMMs from *Mafb*-cKO mice (**Supplementary**
270 **Figure 4**). Thus, we proposed that MAFB in human and murine macrophages has a
271 similar role during *Mtb* infection.
272
273 ***Mafb* deficiency in macrophages increased mortality during *Mtb* infection in mice**
274 To examine whether *Mafb* deficiency in macrophages influences the outcome
275 of *Mtb* infection in mice, we conducted aerosol infections in *Mafb*-cKO mice and WT
276 mice and monitored them for 315 days. We found that *Mafb*-cKO mice started
277 succumbing after 20 weeks, and no *Mafb*-cKO mice survived by the end of the
278 experiment (**Figure 3A**). The survival probability between the two groups was analyzed
279 by Kaplan–Meier analysis and the log-rank test. The median survival of *Mafb*-cKO
280 mice was 211 days, which was significantly shorter than that of WT mice.-We next
281 determined the bacterial burden in the murine organs after *Mtb* infection. At 10 and 20
282 weeks p.i., *Mafb*-cKO mice exhibited significantly higher burden in the lungs, but not at
283 4 weeks p.i. (**Figure 3B**). The spleens of *Mafb*-cKO mice also showed a higher burden
284 at 10 and 20 weeks p.i., demonstrating the involvement of *Mafb* in the control of the

285 bacterial burden in the lung and spleen (**Supplementary Figure 5**).

286

287 **Transcriptomics of *Mtb*-infected *Mafb*-cKO mouse lungs**

288 To investigate whether *Mafb* deficiency in macrophages alters BPs in the lungs
289 during *Mtb* infection, we performed mRNA-seq on the lungs of *Mtb*-infected *Mafb*-cKO
290 and control mice at 10 or 20 weeks p.i., respectively. At 10 weeks p.i., 89 genes were
291 identified as DEGs in the lungs of *Mtb*-infected *Mafb*-cKO mice (**Figure 4A**). Among
292 these 89 genes, 48 genes were upregulated and 41 genes were downregulated. GOBP of
293 DEGs demonstrated that cell–cell adhesion, leukocyte proliferation, or the regulation of
294 T-cell activation were activated, whereas complement activation, cellular response to
295 type II IFN, synapse pruning, and response to protozoan were suppressed in the lungs of
296 *Mafb*-cKO mice (**Figure 4B**). Concept gene network for GO categories visualized that
297 *Cd1d1*, *Cdkn2a*, *Tarm1*, *Havcr2*, and *Slfn1* were the key genes for T-cell regulation
298 (**Figure 4C**). KEGG pathway enrichment analysis demonstrated the enrichment of
299 osteoclast differentiation (**Supplementary Figure 6A**). Complement components such
300 as *C1qa*, *C1qb*, or *C1qc*, identified in suppressed GO categories, played a central role in
301 complement activation. The involvement of *Mafb* in regulating complement
302 components was consistent with the previous report (15). In addition to complement
303 components, downregulated DEGs included cytokine ligands such as *Ccl8*, which is
304 also known as *monocyte chemoattractant protein 2* (MCP2), *Ccl12*, known as *monocyte*
305 *chemoattractant protein 5* (MCP5), or *Pf4,* known as *Cxcl4*. KEGG pathway
306 enrichment analysis demonstrated that complement and coagulation cascade, and
307 chemokine signaling pathway were enriched in downregulated DEGs (**Supplementary**
308 **Figure 6BC**). At 20 weeks p.i., 267 DEGs were identified (**Figure 5A**), of which DEGs

309 found at 10 weeks p.i. were included. Among the 267 genes, 110 genes were
310 upregulated and 157 genes were downregulated. GOBP showed that myeloid leukocyte
311 activation, myeloid leukocyte differentiation, the regulation of macrophage activation,
312 the regulation of endocytosis, and the regulation of angiogenesis were upregulated,
313 whereas leukocyte migration, leukocyte chemotaxis, leukocyte proliferation, and
314 immune response cell-surface receptor-signaling pathway were downregulated in the
315 lungs of *Mtb*-infected *Mafb*-cKO mice (**Figure 5B**). Concept gene network revealed
316 *Csfs* (GM-CSF), a key regulator for macrophage and dendritic cell function, *Mmp8*,
317 *Cd177*, genes associated with neutrophil activation and migration, or *Sirpb1 family* for
318 phagocytosis and immune modulation in upregulated DEGs, highlights strong
319 differentiation and the activation of myeloid-derived immune cells (**Figure 5C**). Down
320 regulated DEGs included *Ccl22*, *Ccl8*, *Ccl5*, *Cx3cr1*, *Pf4*, and *Ccr7*, which are involved
321 in chemokine signaling or leukocyte migration; *P2rx7*, *Nfatc2*, and *Ptpn22*, regulatory
322 genes in T-cell activation and immune tolerance, *Cd22* or *Icosl*, which are involved in B
323 cell-mediated immune response, suggesting reduced adaptive immune activation and
324 leukocyte or lymphocyte recruitment in the lungs of *Mtb*-infected *Mafb*-cKO mice
325 compared to those of control mice (**Figure 5C**).
326

327 **Immune cell recruitment in the lungs of *Mtb*-infected *Mafb*-cKO mice**

328 Transcriptomics of the lungs of *Mtb*-infected *Mafb*-cKO mice suggested altered
329 recruitment of immune cells during *Mtb* infection (**Figure 4 and 5**). Therefore, we
330 investigated the proportion of immune cells in the lungs of *Mafb*-cKO mice during *Mtb*
331 infection by flow cytometry (**Figure 6**). The frequencies of both $CD4^+$ and $CD8^+$ T-cells
332 were high at 10 weeks p.i., and then decreased at 20 weeks p.i. in control mice, whereas

333 they were at the same levels in *Mafb*-cKO mice during infection, suggesting blocked
334 early recruitment of $CD4^+$ and $CD8^+$ T-cells in the infected lungs of *Mafb*-cKO mice in
335 line with the transcriptomic feature of negative T cell regulation at 10 weeks p.i.
336 (**Figure 6**). The frequency of B-cells remained the same from 10 weeks to 20 weeks p.i.
337 in the control mice; however, it decreased in *Mafb*-cKO mice at 20 weeks p.i., which
338 also supports the transcriptomics data. Despite the impaired chemokine signaling, the
339 frequency of neutrophils was significantly higher in *Mafb*-cKO at 10 or 20 weeks p.i.
340 compared to that in control mice. Although the frequency of macrophages was slightly
341 lower in *Mafb*-cKO mice, the difference was not statistically significant due to the high
342 inter-sample variability. Nonetheless, these results indicate that *Mafb* deficiency in
343 macrophages affects the recruitment of various immune cells to the lungs of *Mtb*-
344 infected mice.
345

346 **Discussion**

347 We have demonstrated that *MAFB* deficiency activates oxidative
348 phosphorylation and impairs type I and II IFN responses in *Mtb*-infected human
349 macrophages (14). For a deeper understanding of *MAFB*'s role in *Mtb* infection, we
350 investigated its function using a murine model of myeloid-specific *Mafb* conditional-
351 knockout (*Mafb*-cKO) mice. Transcriptomics of BMMs from *Mafb*-cKO mice revealed
352 that a ROS metabolic process and oxidative phosphorylation were activated, whereas
353 the IFN responses were suppressed during *Mtb* infection (**Figure 2**), which is consistent
354 with our previous results (14). Therefore, we assume that *MAFB* in human and murine
355 macrophages acts similarly in response to *Mtb* infection.

356 We found that BMMs from *Mafb*-cKO mice failed to control intracellular *Mtb*

357 proliferation (**Figure 1**). In fact, *Mtb* infection typically induces the production of ROS
358 in infected macrophages to reduce the intracellular bacterial load (32). However, an
359 imbalance between ROS and antioxidants leads to oxidative stress, which contributes to
360 the onset and progression of pulmonary diseases, including TB (33, 34). In BMMs from
361 *Mafb*-cKO mice, the ROS metabolic process was activated, and its related genes were
362 identified. CYBB, CAMK2B, and ITPR1 were involved in ROS production, and SOD2,
363 GPX3, and CAT were involved in ROS clearance (35). CYBB is the major catalytic
364 subunit of nicotinamide adenine dinucleotide phosphate (NADPH) oxidase, encoding
365 NOX2 that possesses antimicrobial activity against *Mtb* (36). The superoxide dismutase
366 expressed by *Sod2* detoxifies the major ROS to protect host cells from the damage
367 caused by excessive ROS. Paradoxically, the overexpression of *Sod2* promotes the
368 intracellular survival of *Mtb* (37). During *Mtb* infection, genes related to both ROS
369 production and clearance were upregulated in BMMs derived from *Mafb*-cKO mice,
370 implying that BMMs from *Mafb*-cKO mice generate ROS to clear pathogen while
371 maintaining redox balance to prevent self-damage during infection, thereby actively
372 attempting to eliminate the excessive ROS.

373 *Mtb* infection also activates antiviral responses, including the induction of type
374 I IFNs, in infected macrophages (38, 39). During infection, mycobacterial DNA is
375 initially released from the phagosomes into the cytosols, where it is recognized by
376 cyclic GMP-AMP synthase (cGAS), initiating type I IFN production. This recognition
377 triggers the activation of the cGAS-STING-TBK1 cascade and transcription factors
378 IRF3 and IRF7, followed by the production of type I IFNs and other cytokines (40).
379 Activated IRF3 translocates into the nucleus and binds to IFN-stimulated response
380 element (ISRE) in the promoters of type I IFNs and proinflammatory genes for further

381 transcriptional induction (41). It has been shown that IRF3 is essential for downstream
382 genes, such as *Cxcl10* and *Ifit1*, which are induced by IFN-β and IFN-γ (42). In *Mtb*-
383 infected BMMs from *Mafb*-cKO mice, *Tbk1*, *Irf3*, *Irf7*, *Stat1*, *Stat2,* and other genes
384 with ISRE (*Adar*, *Bst2*, *Cxcl10*, *Gbp2*, *Ifit1*, *Ifit2*, *Ifit3*, *Irf7*, *Irf9*, *Isg15*, *Isg20*, *Mx1*,
385 *Mx2*, *Oas2*, *Oas3*, *Rsad2*, *Sp100)* and type I IFNs (*IFNα*, *IFNβ*) were significantly
386 downregulated (**Figure 2**, **Supplementary Figure 7A**), suggesting that *Mafb* can be a
387 positive regulator in the cGAS-STING-TBK1 cascade.

388 In mycobacterial infection, type I IFNs can be detrimental to the host,
389 considering the type I IFN-driven susceptibility in the mouse model carrying the
390 sensitive allele of the *Sst1* locus (43). Contrary to the results of BMMs from *Mafb*-cKO
391 mice, type I IFNs (IFNα) or genes with ISRE were found to be upregulated in *Mtb*-
392 infected *Mafb*-cKO mouse lungs **(Supplementary Figure 7BC)**. This result may
393 explain the increased mortality and higher bacterial burden in the organs of *Mtb*-
394 infected *Mafb*-cKO mice (**Figure 3**). A possible explanation for this higher bacterial
395 burden in BMMs from *Mafb*-cKO mice is weakened lysosome biogenesis demonstrated
396 by a pathway analysis (**Supplementary Figure 1B**, **2**). In addition, genes related to the
397 immune response to the TB pathway were downregulated in *Mafb*-cKO BMMs
398 compared to those in control BMMs (**Supplementary Figure 3**). Together with the
399 imbalanced ROS metabolism, we proposed that *Mafb*-deficient BMMs lack an effective
400 antibacterial response that would contain intracellular *Mtb*.

401 As expected from the failure of *Mtb* containment at a cellular level, *Mafb*
402 depletion in macrophages causes increased mortality and a higher bacterial burden in
403 the organs of *Mtb*-infected mice (**Figure 3**). To gain an insight into the mechanism
404 underlying the susceptibility of *Mafb*-cKO mice, we performed RNA-seq of *Mafb*-cKO

405 mouse lungs. We identified 1223 DEGs by comparing between *Mtb*-infected BMMs
406 from *Mafb*-cKO and control mice. In the lungs of *Mtb*-infected *Mafb*-cKO mice, 89 or
407 267 genes were identified as DEGs at 10 weeks or 20 weeks p.i., respectively. MafB is a
408 transcription factor that binds to Maf recognition elements (MAREs) in gene promoters
409 (8). We obtained MafB ChIP-sequencing data (28) to compare with the DEGs identified
410 in the present study. Among the 1,223 DEGs in *Mtb*-infected *Mafb*-cKO BMMs, 413
411 genes (33.8%) overlapped with MafB target genes, including 175 upregulated and 238
412 downregulated genes (**Table 1).** In the lungs of *Mtb*-infected *Mafb*-cKO mice, 28 DEGs
413 (31.5%) at 10 weeks p.i. and 55 DEGs (20.6%) at 20 weeks p.i. overlapped with MafB
414 target genes, respectively (**Table 1**). The proportion of DEGs directly bound by MafB
415 was comparable between *Mafb*-cKO BMMs and lungs at 10 weeks p.i.; however, this
416 proportion was lower at 20 weeks p.i., despite a greater number of DEGs being
417 detected. This suggests that secondary effects of *Mafb* deficiency may contribute to the
418 increased mortality observed in *Mafb*-cKO mice during the later stage of infection.
419 Transcriptomics of the lungs of *Mtb*-infected *Mafb*-cKO mice displayed
420 activated myeloid-derived immune cells and differentiation (**Figure 4**). This finding is
421 consistent with the reports that low MafB levels activate self-renewal in resident
422 macrophages(28, 44). Vanneste *et al.* exhibited that myeloid-specific *Mafb* deletion
423 increased both the proliferative ability and cell death in macrophages, decreasing
424 number of macrophages in the mouse lungs (45). We also demonstrated a slightly
425 decreased population of $CD64^{+}$ macrophages among immune cells at 10 weeks p.i. but
426 not at 20 weeks p.i. (**Figure 6**). We displayed a significantly higher frequency of
427 neutrophils in *Mafb*-cKO mouse lungs (**Figure 6**). The result is consistent with the
428 necrosis of macrophages and bacillary replication induce neutrophil recruitment (46). In

429 fact, neutrophil accumulation correlates with increased disease severity, suggesting that
430 excessive neutrophils may exacerbate TB pathology (47). *Mtb*-infected *Mafb*-cKO mice
431 displayed a higher bacterial burden at 10 weeks p.i. in the lungs. Neutrophil recruitment
432 is further enhanced by their release of mediators in response to *Mtb* (48). These findings
433 explain that neutrophils can drive further neutrophil recruitment to the lungs of *Mafb*-
434 cKO mice. Kanai *et al.* also demonstrated an increased myeloid-cell infiltration,
435 including neutrophils, in an ischemic acute kidney injury (AKI) model in *Mafb*-cKO
436 mice, suggesting that *Mafb* is involved in myeloid-cell migration both in the site of
437 infection and injury. (49) Considering that *Mafb* regulates thermogenesis in brown
438 adipose tissue in *Mafb*-cKO mice under cold conditions (50), it is suggested that *Mafb*
439 controls various homeostatic functions in macrophages under infections, injuries, or
440 cold conditions.

441 We demonstrated that *Mafb* deficiency in macrophages impaired the cell
442 signaling for leukocyte migration and the recruitment of $CD4^+$ and $CD8^+$ T-cells in the
443 lungs of *Mtb*-infected mice, suggesting weakened adaptive immunity at an early stage
444 of infection. Several studies have shown the importance of macrophage activation by
445 IFN-γ produced from $CD4^+$ T-cells for protective immunity against *Mtb* in mice (51-
446 53). The depletion of $CD4^+$ T-cells leads to increased bacterial loads and increased
447 severity of the infection in *Mtb*-infected C57BL/6 mice (54). In a macaque model, $CD4^+$
448 T-cells display an "innate-like" defense system and serve as master helper cells to
449 recruit other Th-like effector cells, thereby successfully preventing early
450 extrapulmonary *Mtb* dissemination (55).

451 In summary, the present study provides evidence that *Mafb* depletion in
452 myeloid cells not only impairs macrophage bactericidal activity but also disrupts

453 immune cell recruitment, leading to failed bacterial control and higher mortality in *Mtb*-
454 infected mice.
455
456 **Conflict of Interest Statement**
457 The authors declare that the research was conducted in the absence of any
458 commercial or financial relationships that could be construed as a potential conflict of
459 interest.
460
461 **Author Contributions**
462 HH, SS, MHijikata and NK designed the project. HH, SS, HN, and SO
463 performed the experiments. MHamada, and ST provided the experimental materials.
464 HH and SS analyzed the data. HH, SS, MHijikata and NK wrote and revised the
465 manuscript. All authors approved the manuscript.
466
467 **Funding**
468 This study was supported by the Emerging/Re-emerging Infectious Diseases
469 Project of the Japan Agency for Medical Research and Development (JP23wm0225028,
470 JP23gm1610013, JP23fk0108673, JP23fk0108674, JP23fk0108703, JP25fk0108730),
471 and Grants-in-Aid for Scientific Research, Japan Society for the Promotion of Science
472 (20KK0197, 24K10229).
473
474 **Acknowledgement**
475 We thank Dr. Masayuki Umemura from Ryukyu University for valuable
476 discussions and expert advice on flow cytometric analysis. We also thank all our

477 colleagues and staffs at The Research Institute of Tuberculosis, Japan Anti-Tuberculosis
478 Association for technical and administrative support.
479
480 **Figure legends**
481 **Figure 1. Mycobacterial proliferation on *Mafb*-deficient macrophages.**
482 *Mafb*$^{f/f}$::LysM-Cre$^{+/-}$ (*Mafb*-cKO) and *Mafb* $^{f/f}$ (control) bone marrow-derived
483 macrophages (BMMs) were infected with *Mycobacterium tuberculosis* (*Mtb*). At 1, 3,
484 and 7 days postinfection (p.i.), the numbers of the intracellular bacteria were determined
485 by colony forming units (CFUs). *$P < 0.01$ using Welch's t-test, with Holm–Bonferroni
486 correction applied for multiple comparisons.
487
488 **Figure 2. Transcriptomics of *Mtb*-infected *Mafb*-cKO bone marrow-derived**
489 **macrophages (BMMs)**
490 mRNA sequencing (mRNA-seq) of *Mtb*-infected *Mafb*-cKO BMMs was performed.MA
491 plot showing 1223 differentially expressed genes (DEGs) in *Mtb*-infected *Mafb*-cKO
492 BMMs compared to those in *Mtb*-infected *Mafb* $^{f/f}$ control BMMs, marked in red (FDR
493 < 0.01). Each dot represents expressed genes in the sample. Log FC, log fold change.
494 LogCPM, log count per million. (B) Gene Ontology (GO) analysis for upregulated or
495 downregulated DEGs. Enriched GO biological process (BP) categories in *Mtb*-infected
496 *Mafb*-cKO BMMs can be seen. (C) Gene concept networks of the top 3 upregulated
497 (Up) and downregulated (Down) GOBP categories in *Mtb*-infected *Mafb*-cKO BMMs.
498 Upregulated GOBP categories are leukocyte cell–cell adhesion, reactive oxygen species
499 metabolic process, and nucleotide metabolic process, colored in salmon pink.
500 Downregulated GOBP categories are response to virus, defense response to symbiont,

501 and regulation of innate immune response, as shown in blue.

502

503 **Figure 3. Effect of macrophage-specific *Mafb* deficiency on TB susceptibility in**

504 **mice**

505 (A) *Mafb*$^{f/f}$::LysM-Cre$^{+/+}$ (*Mafb*-cKO) mice and wild-type (WT) mice (*n*=9/group) were

506 aerosol- infected with *Mtb*, and their survival was monitored for 315 days. Survival

507 probability between the two groups was analyzed by Kaplan–Meier analysis and the

508 log-rank test. The median survival of *Mafb*-cKO mice was 211 days. Most of the WT

509 mice survived when the experiment was ended. **P* = 0.00011. (B) Bacterial loads in the

510 lungs of *Mtb*-infected *Mafb*$^{f/f}$::LysM-Cre$^{+/-}$ (*Mafb*-cKO) and control mice were

511 determined by CFU at 4, 10, and 20 weeks p.i. Data from individual mice is shown. **P*

512 < 0.01 using Tukey–Kramer test.

513

514 **Figure 4. Transcriptomics of *Mtb*-infected *Mafb*-cKO mouse lung at 10 weeks p.i.**

515 *Mafb*-cKO mice and control mice were aerosol-infected with *Mtb* for 10 weeks. (A) MA

516 plot showing 89 DEGs in *Mtb*-infected *Mafb*-cKO mouse lungs compared to those in

517 *Mtb*-infected control mouse lungs, marked in red (FDR < 0.01). Each dot represents

518 expressed genes in the sample. Log FC, log fold change. LogCPM, log count per

519 million. (B) GO analysis for DEGs. Enriched GOBP categories in *Mtb*-infected *Mafb*-

520 cKO lungs are shown. (C) Gene concept network of the top 3 upregulated (Up) and

521 downregulated (Down) GOBP categories in *Mtb*-infected *Mafb*-cKO mouse lungs.

522 Upregulated GOBP categories include regulation of leukocyte cell–cell adhesion,

523 regulation of T-cell activation, leukocyte cell–cell adhesion, and leukocyte proliferation,

524 colored in salmon pink. Downregulated GOBP categories are defense response to

525 protozoan, response to protozoan, cellular response to type II interferon, synapse
526 pruning, and complement activation, and classical pathway, as shown in blue.
527
528 **Figure 5. Transcriptomics of *Mtb*-infected *Mafb*-cKO mouse lung at 20 weeks p.i.**
529 *Mafb*-cKO mice and control mice were infected with an aerosol of *Mtb* for 20 weeks.
530 (A) MA plot showing 267 DEGs in *Mtb*-infected *Mafb*-cKO mouse lungs in comparison
531 with control mouse lungs marked in red (FDR < 0.01). Each dot represents expressed
532 genes in the sample. Log FC, log fold change. LogCPM, log count per million. (B) GO
533 analysis for DEGs. Enriched GOBP categories in *Mtb*-infected *Mafb*-cKO lungs were
534 shown. (C) Gene concept network of the top 3 upregulated (Up) and downregulated
535 (Down) GOBP categories in *Mtb*-infected *Mafb*-cKO mouse lungs. The upregulated
536 GOBP categories include myeloid leukocyte activation, regulation of endocytosis,
537 myeloid leukocyte differentiation, regulation of angiogenesis, and regulation of
538 macrophage activation colored in salmon pink. Downregulated GOBP categories are
539 leukocyte proliferation, lymphocyte proliferation, immune response cell surface
540 receptor signaling pathway, and leukocyte chemotaxis, shown in blue.
541
542 **Figure 6. Population of immune cells in *Mtb*-infected Mafb-cKO mice**
543 The proportion of the immune cell population in the lungs of *Mtb*-infected *Maf*b-cKO or
544 control mice was determined by flow cytometry at 10 or 20 weeks p.i. The proportions
545 of $CD45^+$, B-cells, neutrophils, macrophages, $CD4^+$ T-cells, $CD8^+$ T-cells, and alveolar
546 macrophages are shown. $*P < 0.05$ using the Wilcox test for each time point.

547 **Table 1. Comparison of MafB ChIP-seq peaks and the DEGs**

548 MafB ChIP-seq peaks are compared with the DEGs identified in *Mtb*-infected *Mafb*-
549 cKO mouse BMMs, *Mtb*-infected *Mafb*-cKO mouse lungs at 10 weeks p.i., or *Mtb*-
550 infected *Mafb*-cKO mouse lungs at 20 weeks p.i. The ChIP-seq data (GEO
551 GSM1964739/SRA SRX1465586) (28) was downloaded via ChIP-Atlas (accessed 27
552 June 2025) (29)

		Upregulated	Downregulated	Total
Mafb-cKO mouse BMMs	DEGs	614	609	1223
	MafB ChIP-seq peaks	175	238	413
		28.5%	39.1%	33.8%
Mafb-cKO mouse lungs, 10w	DEGs	48	41	89
	MafB ChIP-seq peak	14	14	28
		29.2%	34.1%	31.5%
Mafb-cKO mouse lungs, 20w	DEGs	110	157	267
	MafB ChIP-seq peak	24	31	55
		21.8%	19.7%	20.6%

553

References

1. World Health Organization. Global Tuberculosis Report 2024. Geneva: (2024).
2. Dheda K, Migliori GB. New Framework to Define the Spectrum of Tuberculosis. *The Lancet Respiratory Medicine* (2024) 12(6):426-8. doi: 10.1016/S2213-2600(24)00085-7.
3. Frascella B, Richards AS, Sossen B, Emery JC, Odone A, Law I, et al. Subclinical Tuberculosis Disease-a Review and Analysis of Prevalence Surveys to Inform Definitions, Burden, Associations, and Screening Methodology. *Clin Infect Dis* (2021) 73(3):e830-e41. Epub 2020/09/17. doi: 10.1093/cid/ciaa1402.
4. Coleman M, Nguyen TA, Luu BK, Hill J, Ragonnet R, Trauer JM, et al. Finding and Treating Both Tuberculosis Disease and Latent Infection During Population-Wide Active Case Finding for Tuberculosis Elimination. *Front Med (Lausanne)* (2023) 10:1275140. Epub 2023/11/01. doi: 10.3389/fmed.2023.1275140.
5. Gilmour B, Alene KA. Ending Tuberculosis: Challenges and Opportunities. *Frontiers in Tuberculosis* (2024) 2. doi: 10.3389/ftubr.2024.1487518.
6. Schurz H, Naranbhai V, Yates TA, Gilchrist JJ, Parks T, Dodd PJ, et al. Multi-Ancestry Meta-Analysis of Host Genetic Susceptibility to Tuberculosis Identifies Shared Genetic Architecture. *Elife* (2024) 13. Epub 2024/01/15. doi: 10.7554/eLife.84394.
7. Mahasirimongkol S, Yanai H, Mushiroda T, Promphittayarat W, Wattanapokayakit S, Phromjai J, et al. Genome-Wide Association Studies of Tuberculosis in Asians Identify Distinct at-Risk Locus for Young Tuberculosis. *J Hum Genet* (2012) 57(6):363-7. Epub 2012/05/04. doi: 10.1038/jhg.2012.35.
8. Kataoka K, Fujiwara KT, Noda M, Nishizawa M. Mafb, a New Maf Family Transcription Activator That Can Associate with Maf and Fos but Not with Jun. *Mol Cell Biol* (1994) 14(11):7581-91. Epub 1994/11/01. doi: 10.1128/mcb.14.11.7581-7591.1994.
9. Cordes SP, Barsh GS. The Mouse Segmentation Gene Kr Encodes a Novel Basic Domain-Leucine Zipper Transcription Factor. *Cell* (1994) 79(6):1025-34. doi: https://doi.org/10.1016/0092-8674(94)90033-7.
10. Fujino M, Ojima M, Takahashi S. Exploring Large Maf Transcription Factors: Functions, Pathology, and Mouse Models with Point Mutations. *Genes (Basel)* (2023) 14(10). Epub 2023/10/28. doi: 10.3390/genes14101883.
11. Hamada M, Nakamura M, Tran MT, Moriguchi T, Hong C, Ohsumi T, et al. Mafb Promotes Atherosclerosis by Inhibiting Foam-Cell Apoptosis. *Nat Commun* (2014) 5:3147. Epub 2014/01/22. doi: 10.1038/ncomms4147.
12. Kim H, Seed B. The Transcription Factor Mafb Antagonizes Antiviral Responses by Blocking Recruitment of Coactivators to the Transcription Factor Irf3. *Nat Immunol* (2010) 11(8):743-50. Epub 2010/06/29. doi: 10.1038/ni.1897.
13. Simon-Fuentes M, Rios I, Herrero C, Lasala F, Labiod N, Luczkowiak J, et al. Mafb Shapes Human Monocyte-Derived Macrophage Response to Sars-Cov-2 and Controls Severe Covid-19 Biomarker Expression. *JCI Insight* (2023) 8(24). Epub 2023/11/02. doi: 10.1172/jci.insight.172862.
14. Hikichi H, Seto S, Wakabayashi K, Hijikata M, Keicho N. Transcription Factor Mafb Controls Type I and Ii Interferon Response-Mediated Host Immunity in Mycobacterium Tuberculosis-Infected Macrophages. *Front Microbiol* (2022) 13:962306. Epub 2022/11/22. doi: 10.3389/fmicb.2022.962306.
15. Tran MTN, Hamada M, Jeon H, Shiraishi R, Asano K, Hattori M, et al. Mafb Is a Critical Regulator of Complement Component C1q. *Nat Commun* (2017) 8(1):1700.

Epub 20171122. doi: 10.1038/s41467-017-01711-0.
16. Seto S, Tsujimura K, Koide Y. Coronin-1a Inhibits Autophagosome Formation around Mycobacterium Tuberculosis-Containing Phagosomes and Assists Mycobacterial Survival in Macrophages. *Cell Microbiol* (2012) 14(5):710-27. Epub 20120214. doi: 10.1111/j.1462-5822.2012.01754.x.
17. Furuuchi K, Seto S, Nakamura H, Hikichi H, Miyabayashi A, Wakabayashi K, et al. Novel Screening System of Virulent Strains for the Establishment of a Mycobacterium Avium Complex Lung Disease Mouse Model Using Whole-Genome Sequencing. *Microbiol Spectr* (2022) 10(3):e0045122. Epub 20220517. doi: 10.1128/spectrum.00451-22.
18. Nakamura H, Hikichi H, Seto S, Hijikata M, Keicho N. Transcriptional Regulators Sp110 and Sp140 Modulate Inflammatory Response Genes in Mycobacterium Tuberculosis-Infected Human Macrophages. *Microbiol Spectr* (2024) 12(10):e0010124. Epub 2024/08/20. doi: 10.1128/spectrum.00101-24.
19. Weischenfeldt J, Porse B. Bone Marrow-Derived Macrophages (Bmm): Isolation and Applications. *CSH Protoc* (2008) 2008:pdb prot5080. Epub 2008/01/01. doi: 10.1101/pdb.prot5080.
20. Kawai S, Takagi Y, Kaneko S, Kurosawa T. Effect of Three Types of Mixed Anesthetic Agents Alternate to Ketamine in Mice. *Exp Anim* (2011) 60(5):481-7. doi: 10.1538/expanim.60.481.
21. Patro R, Duggal G, Love MI, Irizarry RA, Kingsford C. Salmon Provides Fast and Bias-Aware Quantification of Transcript Expression. *Nat Methods* (2017) 14(4):417-9. Epub 2017/03/07. doi: 10.1038/nmeth.4197.
22. Soneson C, Love MI, Robinson MD. Differential Analyses for Rna-Seq: Transcript-Level Estimates Improve Gene-Level Inferences. *F1000Res* (2015) 4:1521. Epub 2016/03/01. doi: 10.12688/f1000research.7563.2.
23. Robinson MD, McCarthy DJ, Smyth GK. Edger: A Bioconductor Package for Differential Expression Analysis of Digital Gene Expression Data. *Bioinformatics* (2010) 26(1):139-40. Epub 2009/11/17. doi: 10.1093/bioinformatics/btp616.
24. Lun AT, Chen Y, Smyth GK. It's De-Licious: A Recipe for Differential Expression Analyses of Rna-Seq Experiments Using Quasi-Likelihood Methods in Edger. *Methods Mol Biol* (2016) 1418:391-416. Epub 2016/03/24. doi: 10.1007/978-1-4939-3578-9_19.
25. Wu T, Hu E, Xu S, Chen M, Guo P, Dai Z, et al. Clusterprofiler 4.0: A Universal Enrichment Tool for Interpreting Omics Data. *Innovation (Camb)* (2021) 2(3):100141. Epub 2021/09/25. doi: 10.1016/j.xinn.2021.100141.
26. Ge SX, Jung D, Yao R. Shinygo: A Graphical Gene-Set Enrichment Tool for Animals and Plants. *Bioinformatics* (2020) 36(8):2628-9. Epub 2019/12/29. doi: 10.1093/bioinformatics/btz931.
27. Luo W, Brouwer C. Pathview: An R/Bioconductor Package for Pathway-Based Data Integration and Visualization. *Bioinformatics* (2013) 29(14):1830-1. Epub 2013/06/07. doi: 10.1093/bioinformatics/btt285.
28. Soucie EL, Weng Z, Geirsdottir L, Molawi K, Maurizio J, Fenouil R, et al. Lineage-Specific Enhancers Activate Self-Renewal Genes in Macrophages and Embryonic Stem Cells. *Science* (2016) 351(6274):aad5510. Epub 2016/01/23. doi: 10.1126/science.aad5510.
29. Zou Z, Ohta T, Oki S. Chip-Atlas 3.0: A Data-Mining Suite to Explore

Chromosome Architecture Together with Large-Scale Regulome Data. *Nucleic Acids Res* (2024) 52(W1):W45-W53. Epub 2024/05/16. doi: 10.1093/nar/gkae358.
30. Sadee W, Cheeseman IH, Papp A, Pietrzak M, Seweryn M, Zhou X, et al. Human Alveolar Macrophage Response to Mycobacterium Tuberculosis: Immune Characteristics Underlying Large Inter-Individual Variability. *Res Sq* (2023). Epub 2023/06/19. doi: 10.21203/rs.3.rs-2986649/v1.
31. Song Q, Meng B, Xu H, Mao Z. The Emerging Roles of Vacuolar-Type Atpase-Dependent Lysosomal Acidification in Neurodegenerative Diseases. *Transl Neurodegener* (2020) 9(1):17. Epub 2020/05/13. doi: 10.1186/s40035-020-00196-0.
32. Shastri MD, Shukla SD, Chong WC, Dua K, Peterson GM, Patel RP, et al. Role of Oxidative Stress in the Pathology and Management of Human Tuberculosis. *Oxid Med Cell Longev* (2018) 2018:7695364. Epub 2018/11/09. doi: 10.1155/2018/7695364.
33. Zuo L, Wijegunawardana D. Redox Role of Ros and Inflammation in Pulmonary Diseases. *Adv Exp Med Biol* (2021) 1304:187-204. Epub 2021/05/22. doi: 10.1007/978-3-030-68748-9_11.
34. Borbora SM, Satish BA, Sundar S, B M, Bhatt S, Balaji KN. Mycobacterium Tuberculosis Elevates Slit2 Expression within the Host and Contributes to Oxidative Stress Responses During Infection. *J Infect Dis* (2023). Epub 2023/05/09. doi: 10.1093/infdis/jiad126.
35. Su R, Yuan J, Gao T, Liu Y, Shu W, Wang Y, et al. Selection and Validation of Genes Related to Oxidative Stress Production and Clearance in Macrophages Infected with Mycobacterium Tuberculosis. *Front Cell Infect Microbiol* (2023) 13:1324611. Epub 2023/12/27. doi: 10.3389/fcimb.2023.1324611.
36. Yang CS, Shin DM, Kim KH, Lee ZW, Lee CH, Park SG, et al. Nadph Oxidase 2 Interaction with Tlr2 Is Required for Efficient Innate Immune Responses to Mycobacteria Via Cathelicidin Expression. *J Immunol* (2009) 182(6):3696-705. Epub 2009/03/07. doi: 10.4049/jimmunol.0802217.
37. Ren X, Dong W, Feng J, Li P, Zheng Y, Wang G, et al. Mir-495 Regulates Cellular Reactive Oxygen Species Levels by Targeting Sod2 to Inhibit Intracellular Survival of Mycobacterium Tuberculosis in Macrophages. *Infection and Immunity* (2021) 89(12). doi: 10.1128/iai.00315-21.
38. Wassermann R, Gulen MF, Sala C, Perin SG, Lou Y, Rybniker J, et al. Mycobacterium Tuberculosis Differentially Activates Cgas- and Inflammasome-Dependent Intracellular Immune Responses through Esx-1. *Cell Host Microbe* (2015) 17(6):799-810. Epub 2015/06/07. doi: 10.1016/j.chom.2015.05.003.
39. Truong T, Martin K, Salemi M, Ray A, Phinney BS, Penn BH. The Balance between Antiviral and Antibacterial Responses During M. Tuberculosis Infection Is Regulated by the Ubiquitin Ligase Cbl. *bioRxiv* (2024). Epub 2024/05/27. doi: 10.1101/2024.05.15.594178.
40. Cheng Y, Schorey JS. Mycobacterium Tuberculosis-Induced Ifn-Beta Production Requires Cytosolic DNA and Rna Sensing Pathways. *J Exp Med* (2018) 215(11):2919-35. Epub 2018/10/20. doi: 10.1084/jem.20180508.
41. Dalskov L, Narita R, Andersen LL, Jensen N, Assil S, Kristensen KH, et al. Characterization of Distinct Molecular Interactions Responsible for Irf3 and Irf7 Phosphorylation and Subsequent Dimerization. *Nucleic Acids Res* (2020) 48(20):11421-33. Epub 2020/11/19. doi: 10.1093/nar/gkaa873.
42. Tong Z, Zou JP, Wang SY, Luo WW, Wang YY. Activation of the Cgas-Sting-

Irf3 Axis by Type I and Ii Interferons Contributes to Host Defense. *Adv Sci (Weinh)* (2024) 11(35):e2308890. Epub 2024/07/15. doi: 10.1002/advs.202308890.
43. Ji DX, Yamashiro LH, Chen KJ, Mukaida N, Kramnik I, Darwin KH, et al. Type I Interferon-Driven Susceptibility to Mycobacterium Tuberculosis Is Mediated by Il-1ra. *Nat Microbiol* (2019) 4(12):2128-35. Epub 2019/10/16. doi: 10.1038/s41564-019-0578-3.
44. Bird L. Self-Renewing Macrophages. *Nature Reviews Immunology* (2009) 9(12):822-. doi: 10.1038/nri2678.
45. Vanneste D, Bai Q, Hasan S, Peng W, Pirottin D, Schyns J, et al. Mafb-Restricted Local Monocyte Proliferation Precedes Lung Interstitial Macrophage Differentiation. *Nat Immunol* (2023) 24(5):827-40. Epub 2023/03/18. doi: 10.1038/s41590-023-01468-3.
46. Repasy T, Martinez N, Lee J, West K, Li W, Kornfeld H. Bacillary Replication and Macrophage Necrosis Are Determinants of Neutrophil Recruitment in Tuberculosis. *Microbes Infect* (2015) 17(8):564-74. Epub 2015/04/12. doi: 10.1016/j.micinf.2015.03.013.
47. Parker HA, Forrester L, Kaldor CD, Dickerhof N, Hampton MB. Antimicrobial Activity of Neutrophils against Mycobacteria. *Front Immunol* (2021) 12:782495. Epub 2022/01/11. doi: 10.3389/fimmu.2021.782495.
48. Lowe DM, Redford PS, Wilkinson RJ, O'Garra A, Martineau AR. Neutrophils in Tuberculosis: Friend or Foe? *Trends Immunol* (2012) 33(1):14-25. Epub 2011/11/19. doi: 10.1016/j.it.2011.10.003.
49. Kanai M, Nishino T, Daassi D, Kimura A, Liao CW, Javanfekr Shahri Z, et al. Mafb in Macrophages Regulates Prostaglandin E2-Mediated Lipid Mediator Class Switch through Alox15 in Ischemic Acute Kidney Injury. *J Immunol* (2024) 213(8):1212-24. Epub 2024/09/04. doi: 10.4049/jimmunol.2300844.
50. Yadav MK, Ishida M, Gogoleva N, Liao CW, Salim FN, Kanai M, et al. Mafb in Macrophages Regulates Cold-Induced Neuronal Density in Brown Adipose Tissue. *Cell Rep* (2024) 43(4):113978. Epub 2024/03/24. doi: 10.1016/j.celrep.2024.113978.
51. Scanga CA, Mohan VP, Yu K, Joseph H, Tanaka K, Chan J, et al. Depletion of Cd4(+) T Cells Causes Reactivation of Murine Persistent Tuberculosis Despite Continued Expression of Interferon Gamma and Nitric Oxide Synthase 2. *J Exp Med* (2000) 192(3):347-58. Epub 2000/08/10. doi: 10.1084/jem.192.3.347.
52. Mogues T, Goodrich ME, Ryan L, LaCourse R, North RJ. The Relative Importance of T Cell Subsets in Immunity and Immunopathology of Airborne Mycobacterium Tuberculosis Infection in Mice. *J Exp Med* (2001) 193(3):271-80. Epub 2001/02/07. doi: 10.1084/jem.193.3.271.
53. Caruso AM, Serbina N, Klein E, Triebold K, Bloom BR, Flynn JL. Mice Deficient in Cd4 T Cells Have Only Transiently Diminished Levels of Ifn-Gamma, yet Succumb to Tuberculosis. *J Immunol* (1999) 162(9):5407-16. Epub 1999/05/05.
54. Flory CM, Hubbard RD, Collins FM. Effects of in Vivo T Lymphocyte Subset Depletion on Mycobacterial Infections in Mice. *J Leukoc Biol* (1992) 51(3):225-9. Epub 1992/03/01. doi: 10.1002/jlb.51.3.225.
55. Canaday DH, Wilkinson RJ, Li Q, Harding CV, Silver RF, Boom WH. Cd4(+) and Cd8(+) T Cells Kill Intracellular Mycobacterium Tuberculosis by a Perforin and Fas/Fas Ligand-Independent Mechanism. *J Immunol* (2001) 167(5):2734-42. Epub 2001/08/18. doi: 10.4049/jimmunol.167.5.2734.

Fig 1

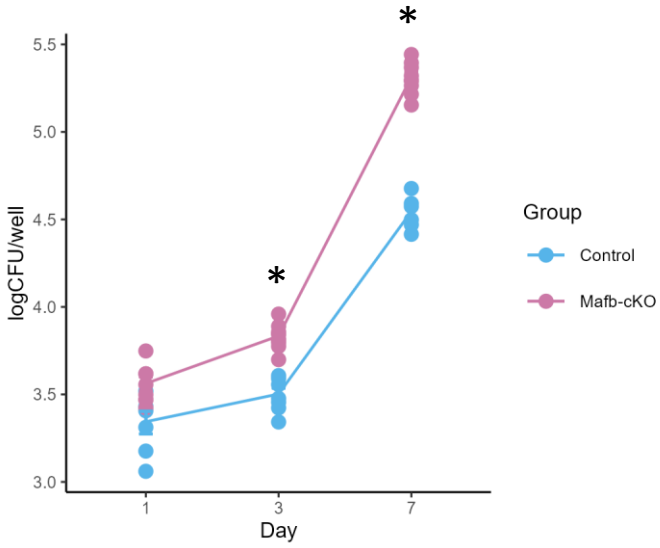

Fig 2

A

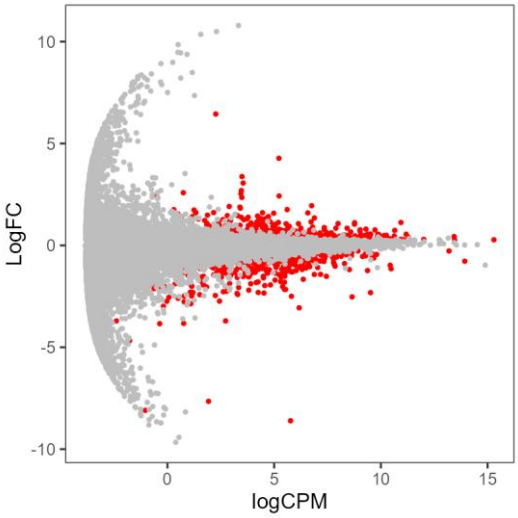
LogFC
logCPM
10
5
0
-5
-10
0
5
10
15

B

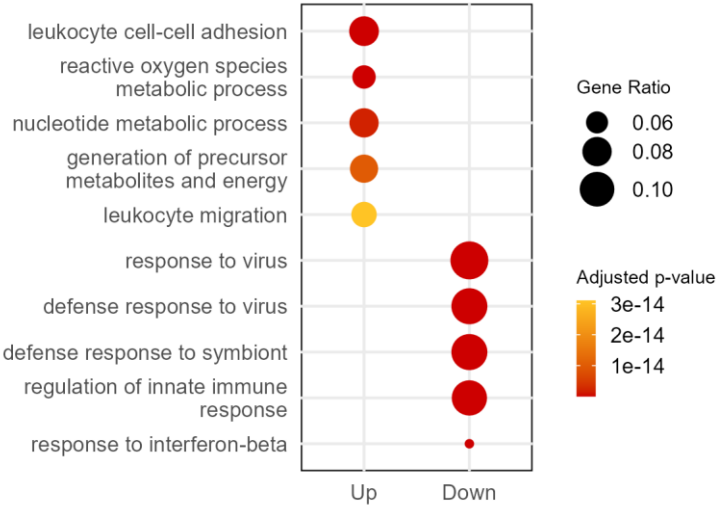
leukocyte cell-cell adhesion
reactive oxygen species metabolic process
nucleotide metabolic process
generation of precursor metabolites and energy
leukocyte migration
response to virus
defense response to virus
defense response to symbiont
regulation of innate immune response
response to interferon-beta
Up
Down
Gene Ratio
0.06
0.08
0.10
Adjusted p-value
3e-14
2e-14
1e-14

C

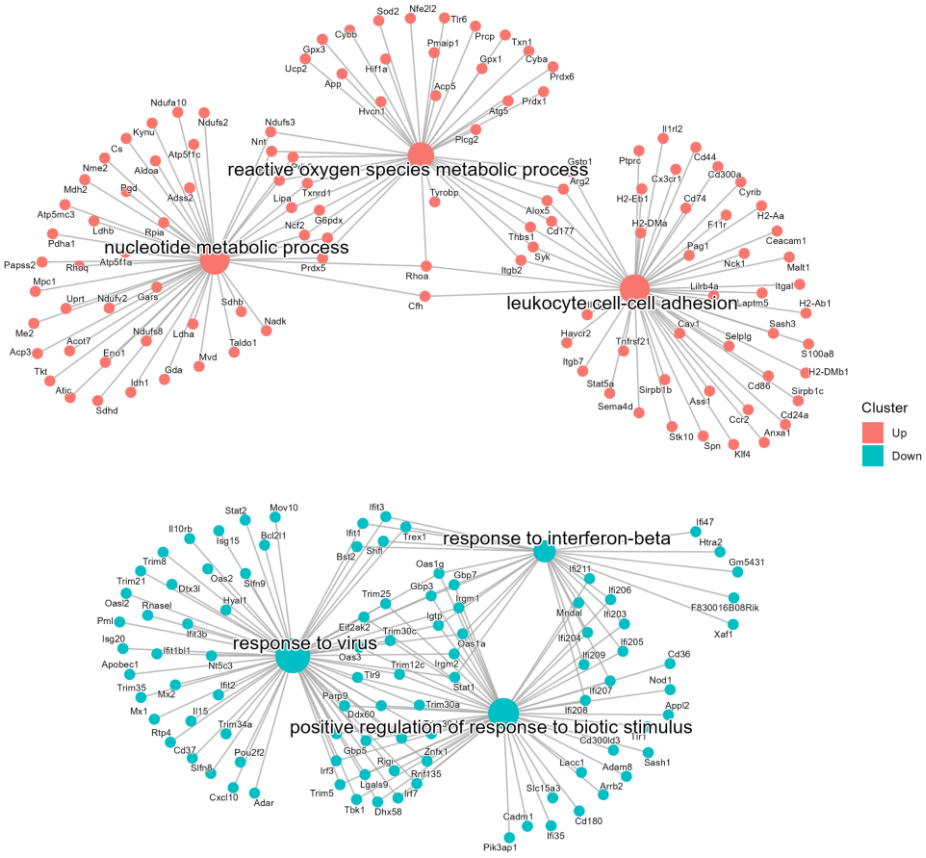
reactive oxygen species metabolic process
nucleotide metabolic process
leukocyte cell-cell adhesion
response to interferon-beta
response to virus
positive regulation of response to biotic stimulus
Cluster
Up
Down

Fig 3

A

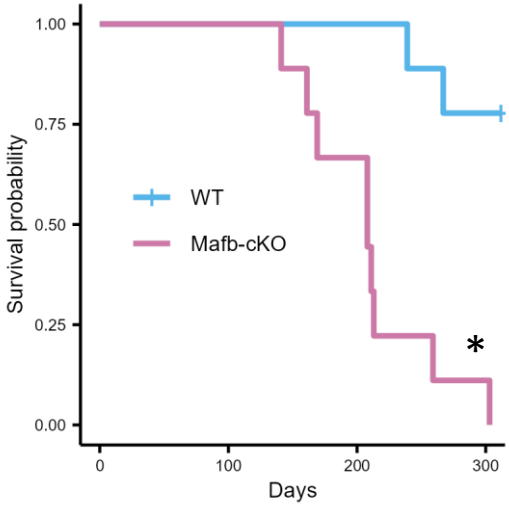
1.00
0.75
0.50
0.25
0.00
Survival probability
WT
Mafb-cKO
*
0
100
200
300
Days

B

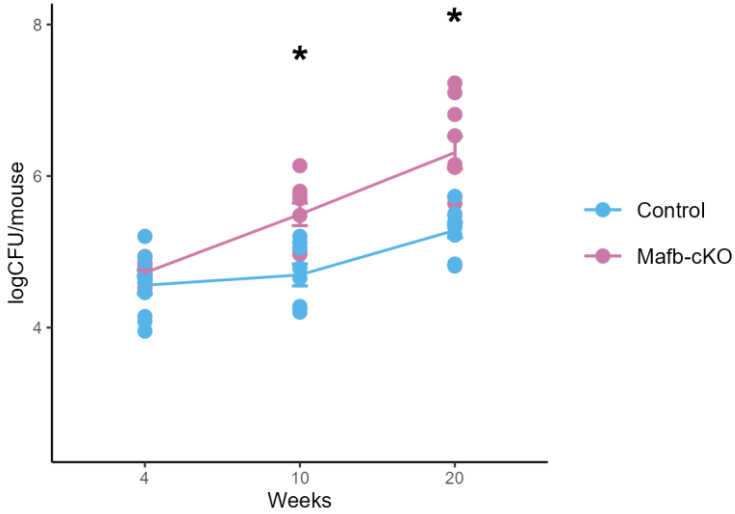
8
6
4
logCFU/mouse
*
*
4
10
20
Weeks
Control
Mafb-cKO

Fig 4

A

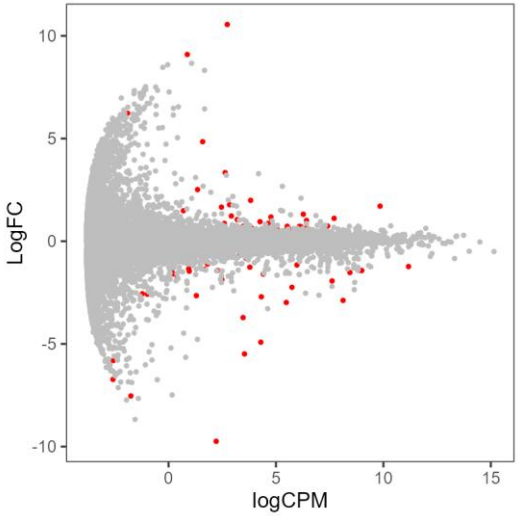
LogFC
logCPM
10
5
0
-5
-10
0
5
10
15

B

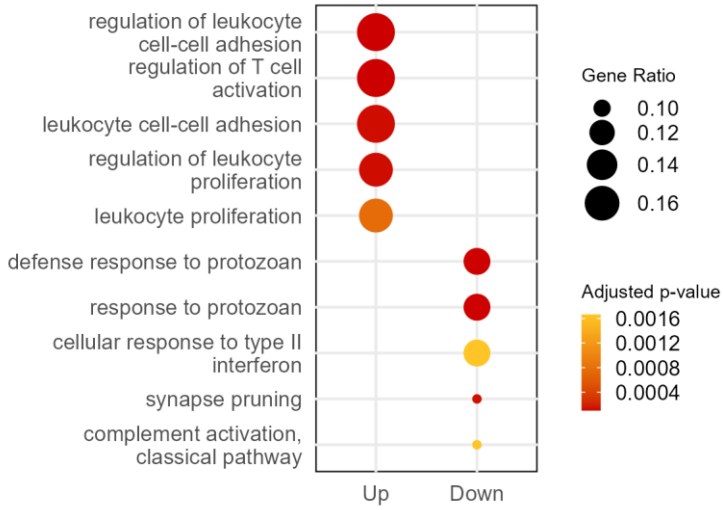
regulation of leukocyte cell-cell adhesion
regulation of T cell activation
leukocyte cell-cell adhesion
regulation of leukocyte proliferation
leukocyte proliferation
defense response to protozoan
response to protozoan
cellular response to type II interferon
synapse pruning
complement activation, classical pathway
Up
Down
Gene Ratio
0.10
0.12
0.14
0.16
Adjusted p-value
0.0016
0.0012
0.0008
0.0004

C

C1qb
synapse pruning
complement activation, classical pathway
C1qc
C1qa
Sirpb1b
Sirpb1a
Sirpb1c
regulation of T cell activation
regulation of leukocyte cell-cell adhesion
leukocyte cell-cell adhesion
Cd1d1
Cdkn2a
Tarm1
Havcr2
Slfn1
leukocyte proliferation
regulation of leukocyte proliferation
Csf2ra
Ocstamp
Cluster
Up
Down
Ccl8
Ccl12
cellular response to type II interferon
Arg1
response to protozoan
Gbp2b
defense response to protozoan
Tspan32
Pf4

Fig 5

A

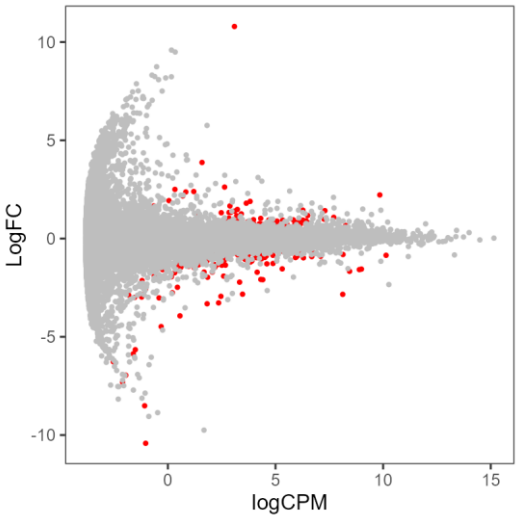
LogFC
logCPM
10
5
0
-5
-10
0
5
10
15

B

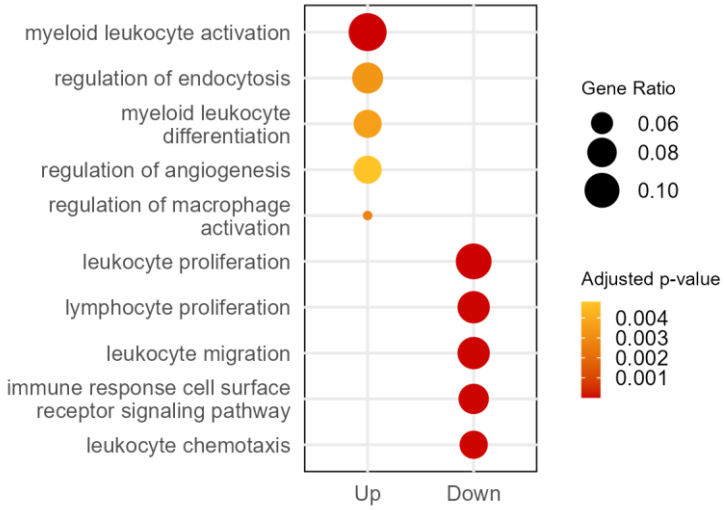
myeloid leukocyte activation
regulation of endocytosis
myeloid leukocyte differentiation
regulation of angiogenesis
regulation of macrophage activation
leukocyte proliferation
lymphocyte proliferation
leukocyte migration
immune response cell surface receptor signaling pathway
leukocyte chemotaxis
Up
Down
Gene Ratio
0.06
0.08
0.10
Adjusted p-value
0.004
0.003
0.002
0.001

C

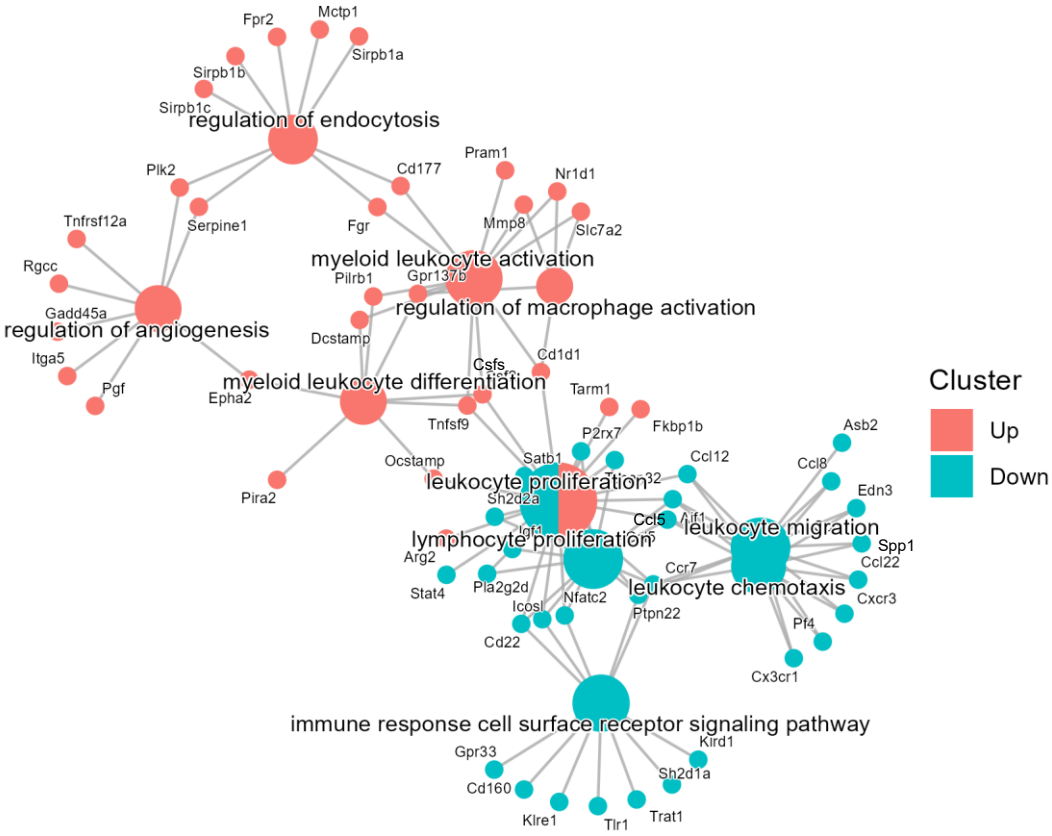
regulation of endocytosis
myeloid leukocyte activation
regulation of angiogenesis
regulation of macrophage activation
myeloid leukocyte differentiation
leukocyte proliferation
lymphocyte proliferation
leukocyte migration
leukocyte chemotaxis
immune response cell surface receptor signaling pathway
Fpr2
Mctp1
Sirpb1a
Sirpb1b
Sirpb1c
Plk2
Serpine1
Cd177
Fgr
Pram1
Nr1d1
Mmp8
Slc7a2
Tnfrsf12a
Rgcc
Gadd45a
Itga5
Pgf
Pilrb1
Gpr137b
Dcstamp
Epha2
Csfs
Cd1d1
Tarm1
Tnfsf9
P2rx7
Fkbp1b
Ocstamp
Satb1
Ccl12
Pira2
Sh2d2a
Ccl5
Aif1
Igf1
Arg2
Stat4
Pla2g2d
Icosl
Nfatc2
Ccr7
Ptpn22
Cd22
Asb2
Ccl8
Edn3
Spp1
Ccl22
Cxcr3
Pf4
Cx3cr1
Gpr33
Cd160
Klre1
Tlr1
Trat1
Sh2d1a
Kird1
Cluster
Up
Down

Fig 6

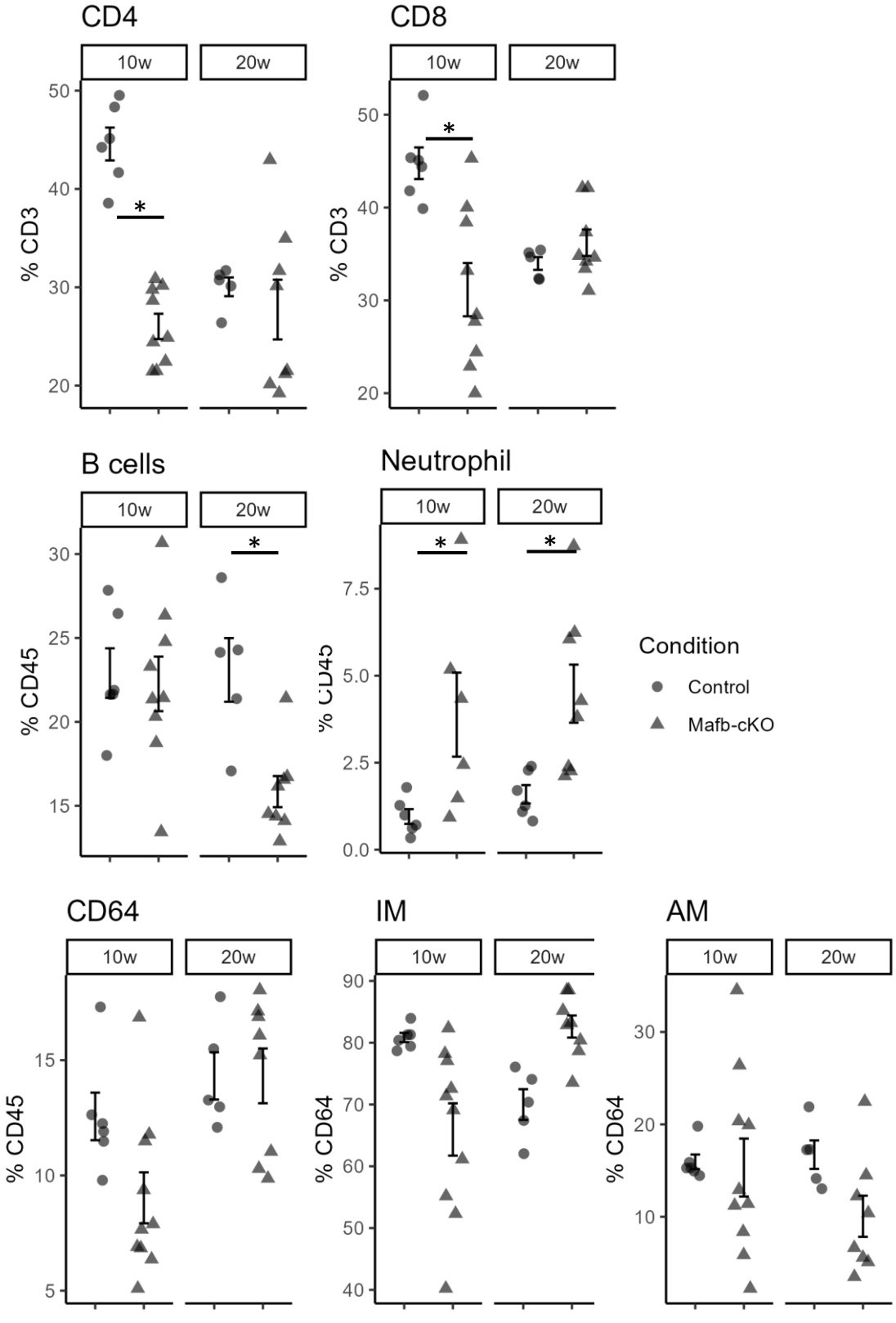
CD4
CD8
B cells
Neutrophil
CD64
IM
AM
10w
20w
% CD3
% CD45
% CD64
Condition
Control
Mafb-cKO